Fractal nature of π-bonded nanocrystalline clusters: A N^+ beam-induced phenomenon in poly(2,6-dimethyl-1,4-phenylene oxide)

A. Das
Department of Chemistry, Indian Institute of Technology, Madras, Chennai-600 036, India

S. Dhara
Materials Science Division, Indira Gandhi Centre for Atomic Research, Kalpakkam-603 102, India

A. Patnaik
Department of Chemistry, Indian Institute of Technology, Madras, Chennai-600 036, India

(Received 8 July 1998)

Formation of nanosized carbonaceous clusters has been investigated in 100 keV N^+ irradiated poly(2,6-dimethyl-1,4-phenylene oxide) [PPO] thin films, using Fourier transform (FT)-Raman, transmission electron microscopy and UV-Vis spectroscopy in the fluence range of $1\times10^{15}-5\times10^{16}$ ions/cm^2. Above a critical fluence of $\sim1\times10^{16}$ ions/cm^2, the energy density transferred to the implanted layer resulted in a molecular construction/self-organization process with the evolution of graphitelike clusters of varying size $\sim2-50$ nm. Electron diffraction analysis of these clusters shows a close resemblance to the formation of single crystalline graphite phase with a zone axis $\langle 070\rangle$. The deduced band gaps from the optical spectra using Tauc's approximation provided information on the electronic structure of the fused hexagonally clustered aromatic rings with varying sizes; the number of the rings varying from $\sim20-170$. Evidence for the signature of fractal patterns, with dimension 1.37 ± 0.02, during aggregation of small particlelike clusters in the polymer implanted layer is presented; analysis of the data suggests the growth process to follow a diffusion-limited-aggregation model. [S0163-1829(99)05715-X]

I. INTRODUCTION

The onset of electronic conductivity and optical blackening in the ion-implanted polymers are attributed to the formation of carbonaceous matrix along the latent track of energetic ions upon a threshold energy density deposition.[1] It has been proposed[2–6] that the small spherical carbon-enriched clusters of $\sim10-50$ nm diameter at separations of $\sim0.1-20$ nm are the carriers of electronic conductivity in the implanted polymers between which the charge carriers tunnel or hop. The propositions made to the fulfill these models were that the conducting clusters were embedded in an insulating matrix with minimum cluster to cluster separation for attainment of a high hopping probability. The carbon enriched material was reported to consist of graphite platelets or highly carbon rich organic matter; the suggested structures ranged from amorphous to single crystalline material.[3] The best model appeared to be that of amorphous hydrogenated carbons[7] (*a*-C:H) where the graphitic components are linked together by different types of polymeric bonds in a dielectric matrix. The diamondlike (DLC) or graphitelike (GLC) nature of the carbon enriched zone is reported to be present depending on the predominant role of either nuclear or electronic modes of energy loss, respectively, as a function of incident ion energy.[1]

The signature of ion beam-induced cluster formation was detected, for the first time, with the help of neutron diffraction technique in the 50 MeV boron-implanted Mylar.[3] Cluster formation due to the ion implantation in polyethylene and polypropylene[4] has been studied by small angle x-ray diffraction (XRD), through Raman spectroscopy[5] and UV-VIS studies.[8] The ion-irradiated films were compared with a-C:H (Refs. 7 and 9) and cluster sizes evaluated using the model proposed by Robertson and O'Reilly[10] and based on the optical band gap, were found to be 3-20 nm. In this model, graphitelike carbon (sp^2 bonding) plays a crucial role in regulating the electronic properties of the material through the π-bonding electrons whereas the sp^3 bonding forms the cross-linked material. Clustering occurs since the sp^2 sites have free π-electrons that tend to agglomerate into graphitelike structures/clusters.[11] Raman spectroscopy has been employed to study the bonding nature of the carbonaceous material of implanted polymers.[5,12] Indirect measurement of cluster size and intercluster distances from temperature-dependent conductivity measurements have also been reported by a number of researchers.[13]

But the accuracy of the clusters data gained by the above mentioned indirect techniques is dependent on the corresponding theories and therefore, these techniques have their own limitations. However, in a direct method, the presence of carbon-enriched zone[11] has been observed using transmission electron microscopy (TEM) in the ion-irradiated polymer. A three-dimensional (3D) network of cross-linked polymer is assumed as a result of ion irradiation and consequently the solubility of the implanted material becomes difficult. No serious effort has been made to explore the crystalline nature of these clusters and their growth except the recent report on microcrystallinity in the proton bombarded poly vinyl chloride, which has been studied with the help of TEM (Ref. 6) analysis.

The mechanism of the electrical conductivity and spin diffusion in ion-irradiated polymers by using a fractal for-

malism was discussed.[14] The variable range hopping (VRH) process was reported to be governed by the interaction of electrons with the phonons of the fractal framework. The fractal concept plays an increasingly important role in the interpretation of phenomena occurring at grain boundaries and in the embedded aggregates. The diffusion-limited aggregation (DLA) model[15,16] in describing fractal growth in materials has been successfully adopted. As a matter of fact, DLA model proposed by Meakin,[16] has been adopted for two-dimensional growth of fractal patterns in the ion-irradiated Ni-Zr (Ref. 17) film where the driving force for the pattern formation has been ascribed to the seeding of small crystal clusters formed during the energy transfer of incident energetic ions. So far no clear experimental evidences, to the authors' knowledge, have been reported on the fractal aggregation of the carbonaceous particles in the irradiated polymers.

Poly(2,6-dimethyl-1,4-phenylene oxide) [PPO], an engineering thermoplastic, is used widely as electrical insulator. In a previous report,[18] we have observed $\sim 13-14$ orders of enhancement in electrical conductivity as induced by 100 keV N^+ implantation on PPO as a function of fluence. Fourier transform (FT)-Raman spectroscopic studies clearly indicated the formation of graphitelike carbon (GLC), which in turn, supports the enhancement of the conductivity in the semiconducting range. The temperature-dependent conductivity measurements showed the presence of the 3D VRH mechanism following the Mott's equation rather than thermally activated band conduction. In this report, microstructural features of the 100 keV N^+ ion-implanted polymer, evidenced by TEM and microdiffraction studies, respectively, are discussed in detail. The evolution of clusters and structural correlation with graphitic materials as a function of fluence are substantiated using FT-Raman and UV-Vis spectroscopic studies along with TEM analysis. Further, experimental evidences of the formation of fractal aggregates of nanosized single crystalline clusters in an amorphous background in the implanted layer is also presented.

II. EXPERIMENT

Thin films of PPO [Mol. Wt. 40 000, Aldrich Co. (USA)] were prepared on fused quartz and cleaved crystalline NaCl substrates at room temperature by the spin coating method from a solution of PPO in $CHCl_3$. Films grown on quartz were used for UV-Vis and Raman spectroscopic measurements and films on NaCl substrate were chosen for the TEM studies. The projected range of 100 keV N^+ ions in this polymer was found to be 320 nm; accordingly, the thickness of the films were maintained at ~ 400 nm for optical studies. Growth and structural evolution of these films were reported earlier.[19] Thin films of PPO were bombarded with 100 keV N^+ with a beam current 1μA under the vacuum of 1×10^{-6} mbar.

FT-Raman (BRUKER FAR 106 Module) profiles were acquired in the wave-number range of 100–3500 cm^{-1} using a Nd:YAG laser of 200 mW power. Analytical transmission electron microscopy (Philips CM200 along with EDAX detector with super ultrathin window) has been used to study the morphology and crystal structure of the pristine and the ion-irradiated samples. Crystalline nature of these clusters are probed by microdiffraction method with a probe diameter of 75 nm. The optical absorption spectra of the as-deposited and bombarded samples coated on quartz were recorded using UV-VIS-NIR spectrometer (Shimadzu PC3101).

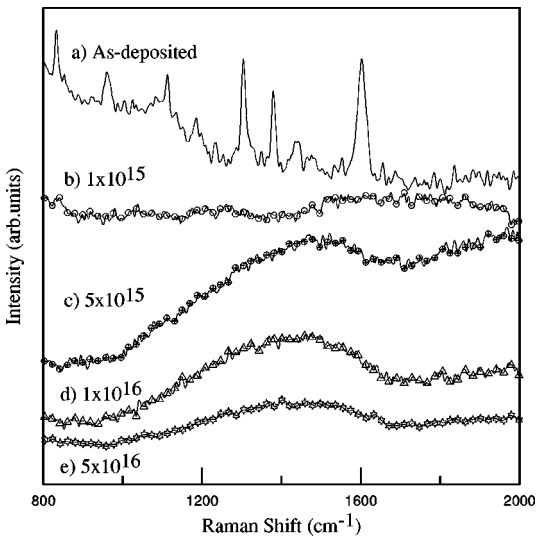

FIG. 1. Raman spectra of as-deposited and implanted PPO films with 100 keV N^+ ions at various fluences.

III. RESULTS AND DISCUSSIONS

PPO, widely used as electrical insulator, is transformed into a highly conducting material due to 100 keV N^+ implantation. The conductivity enhanced by 13 orders of magnitude above a fluence of 10^{16} ions/cm^2, as discussed in our previous report.[18] The induced conductivity associated with an otherwise carbon-enriched matrix, the *a*-C:H, is envisaged to be dependent on the characteristic energy-loss mode during the ion-atom interactions. The Monte Carlo TRIM code[20] calculation revealed the inelastic loss of N^+ ions to be 28.58 eV/Å at 100 keV with an elastic energy loss of 4.73 eV/Å at 100 keV through nuclear interactions with the film constituents.

A. Microstructural elucidation of the N^+ ion-implanted PPO film

1. FT-Raman spectroscopy

In order to achieve considerable information on local bonding nature in the implanted layer, FT-Raman spectra of the pristine film as well as the implanted ones were acquired for different fluences in Fig. 1. The peaks of pristine film [cf. Fig. 1(a)] were assigned at 1603 cm^{-1} for -C-C- mode of the phenyl ring, 1438 and 1347 cm^{-1} for the deformation of CH_3 group and 1231 cm^{-1} due to CH_3-C mode of the substituted methyl group on the benzene ring.[19] The Raman active peak at 1186 cm^{-1} is assigned to C-H bending mode of the ring and the strong maximum at 1112 cm^{-1} due to CH_3-C mode of the methyl group present on the ring. The peak at 832 cm^{-1} is due to C-C stretch mode of the ring. After bombardment, the original peaks of PPO are completely lost and a broad feature is observed at $\sim 1400 - 1500$ cm^{-1} beyond a fluence of 10^{15} ions/cm^2. Upon deconvolution of each experimental curve, as shown in Figs.

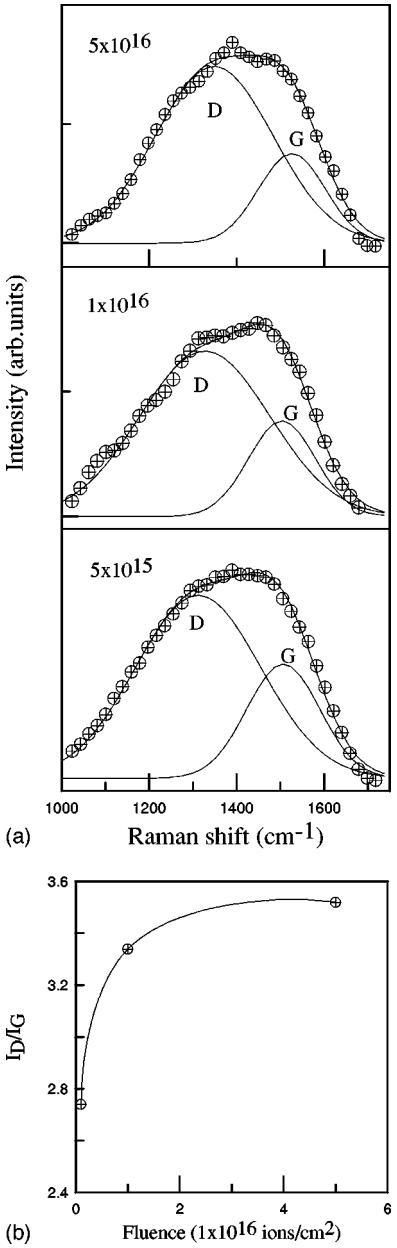

FIG. 2. (a) Deconvoluted Raman spectra of PPO films implanted with 100 keV N^+ ions at various fluences, (b) ratios of the integrated intensities of the *D* and *G* lines in deconvoluted Raman spectra as a function of fluence.

2(a), we find the intensity ratio of *D* band to *G* band is raised. The change in ratio is plotted against the increment in fluence and shown in Fig. 2(b). According to the momentum conservation selection rule, a Raman band at 1580 cm^{-1}, known as *G* band, is observed in graphite with large microcrystals.[21] Raman spectra of graphite and disordered carbons show an additional peak at 1360 cm^{-1}, known as *D* line. This *D* line is attributed to phonons near the Brillouin zone boundary active in small crystallites or on the boundaries of large crystallites. Both bands are found to be present in amorphous carbons and hydrogenated amorphous carbons. The linewidth of both bands is related to the bond-angle distortion and to the presence of relative amount of crystallites in the amorphous matrix. It is reported that both coordinates of carbon, i.e., threefold (sp^2 hybridization) and fourfold (sp^3 hybridization) and bond-angle distortion produce a shift of peaks to lower frequencies. For instance, the *G* line is shifted to 1528 cm^{-1} when the bond angle is changed from the ideal 120° to the disordered average of 117.7° estimated through computer simulation.[22] The shift in *G* line in our experiments, from 1592 cm^{-1} to 1528 cm^{-1} is thus attributed to the bond-angle distortion induced by ion irradiation and the increase in I_D/I_G is interpreted as growth of the graphitic crystallites in size and/or in number density. Therefore, the results of Raman spectroscopy suggest emergence of N^+ ion-induced graphitelike crystals in the implanted layer. The increase in I_D/I_G ratio is also reported for ion-irradiated polystyrene.[12]

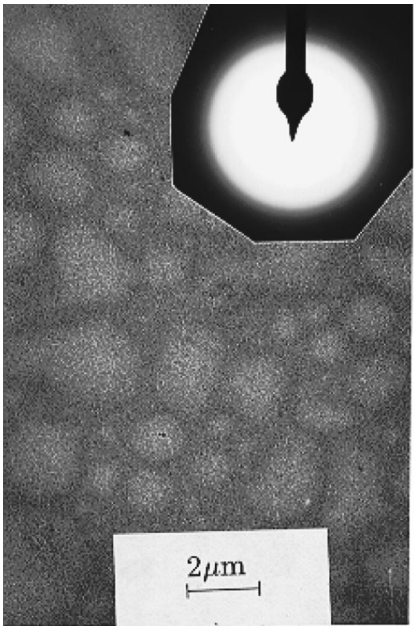

FIG. 3. Bright field transmission electron micrograph of the as-deposited PPO film showing honeycomblike microstructural features. Microdiffraction pattern of the amorphous matrix is shown in the inset.

B. Transmission electron microscopy

1. Imaging of the as-deposited PPO film

For the as-deposited film, coated with ~5 nm Au for charge dispersion, a honeycomb structure was observed in the bright field image of the TEM (Fig. 3). The microstructural features might have arisen due to the nonuniformity in the film thickness induced by nonuniform evaporation of $CHCl_3$ during film preparation. The roughness of the as-deposited film surface on *c*-Si was found to be ~120 Å as estimated with the help of atomic force microscopy. Microdiffraction studies of the as-deposited films at different locations showed broad, diffuse ring pattern (inset of Fig. 3) which is the characteristic of the formation of an amorphous phase. Presence of the amorphous phase in the as-deposited spin casted film, as indicated by XRD studies, has also been reported earlier.[19] 34% crystalline PPO powder was dissolved in $CHCl_3$ for growing thin films. The structural transformation of crystalline PPO powder to ~100% amorphous

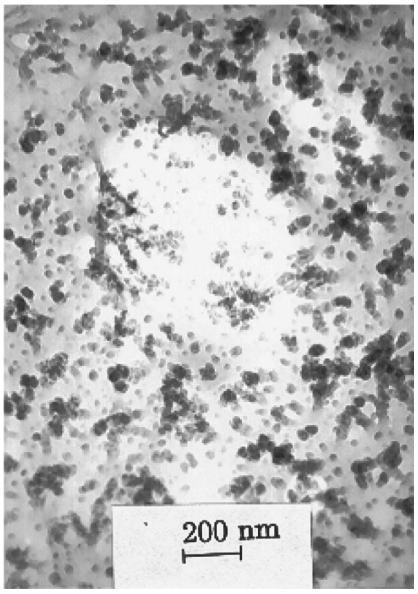

FIG. 4. Ramified growth of carbonaceous clusters shown in the bright field transmission electron micrograph of the PPO film implanted at a fluence of 1×10^{15} ions/cm^2.

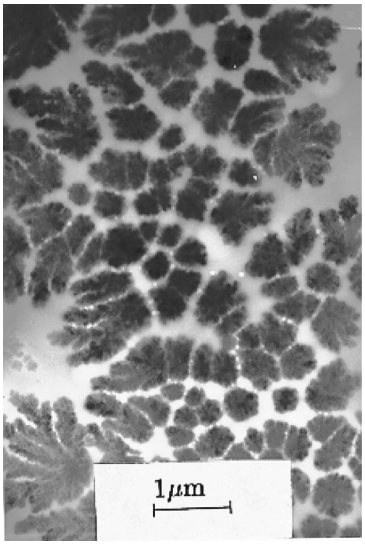

FIG. 5. Bright field transmission electron micrograph of the 100 keV N^+ implanted PPO film indicating growth of carbonaceous clusters in a fractal pattern at a fluence of 1×10^{16} ions/cm^2.

film is explained as a result of possible conformational change on the $CHCl_3$ solvated monomer skeleton.[19]

2. Imaging of the PPO film irradiated with 1×10^{15} *ions/cm*^{2}

TEM image of the 100 keV N^+ ion irradiated at a fluence of 1×10^{15} ions/cm^2 showed clearly the presence of two separate phases. The growth of ramified fractal patterns was surrounded by a featureless structure as shown in the bright field image (Fig. 4). A large number of clusters are distributed in a matrix that upon overlapping have arranged to give rise to the possible fractal pattern. The cluster sizes as measured from the images are found to vary in the range of $\sim2-15$ nm.

3. Imaging of the PPO film irradiated with 1×10^{16} *ions/cm*^{2}

Increasing the ion fluence to 1×10^{16} ions/cm^2, greater deposition of inelastic energy results in further increase in the number density of the above mentioned clusters in the irradiated film. In addition, there is an increase in their size throughout the PPO films. The fractal pattern of the implanted film at a fluence of 1×10^{16} ions/cm^2 is almost obvious in the bright field image of TEM (Fig. 5). At this fluence, coexistence of carbonaceous matrix along with newly grown fractal patterns are also visible in the bright field image of TEM (Fig. 6). Interestingly, black particles, the so-called clusters are seen inside the fractal pattern as shown in the amplified microstructures [Figs. 7(a) and 7(b)]. Figure 7(a) shows cross linking of the clustered regions among each other while in Fig. 7(b) individual clusters inside a single branch of the fractal pattern are evident. The cluster sizes at this fluence are measured to vary from 3 to 25 nm in the irradiated film.

4. Imaging of the PPO film irradiated with 5×10^{16} *ions/cm*^{2}

With further increase in the irradiation fluence to 5×10^{16} ions/cm^2, size of the fractal patterns enhanced ($\sim5-6$ μm) further (Fig. 8) with respect to that for the film implanted with lower fluence. Figure 9 shows the amplified micrograph to that of the previous figure. Figure 10 shows darkfield image of the selected zone grown with fractal patterns. This image shows the assembly of islands of cluster. The cluster sizes varied from as small as ~3 nm to maximum ~50 nm. Average size as well as the number density of these clusters were found to increase with increasing fluence indicating enhanced amount of carbon condensation with increasing fluence. Microdiffraction pattern (outset of Fig. 9) of these clusters clearly shows the single crystalline nature. Structural analysis of these crystalline particles was found to be close to that of graphitic carbon and the zone

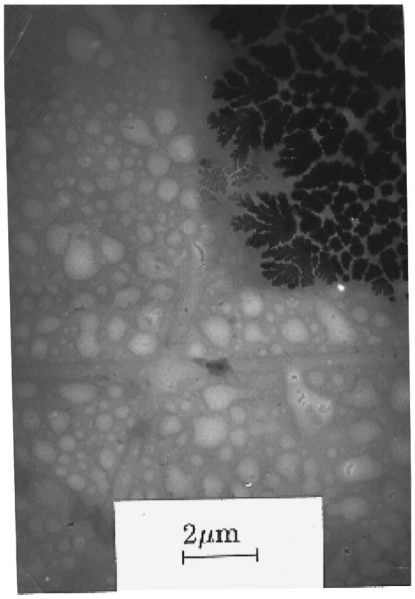

FIG. 6. Bright field transmission electron micrograph of the PPO film implanted at a fluence of 1×10^{16} ions/cm^2 showing the coexistence of featureless matrix and clusters in fractal pattern.

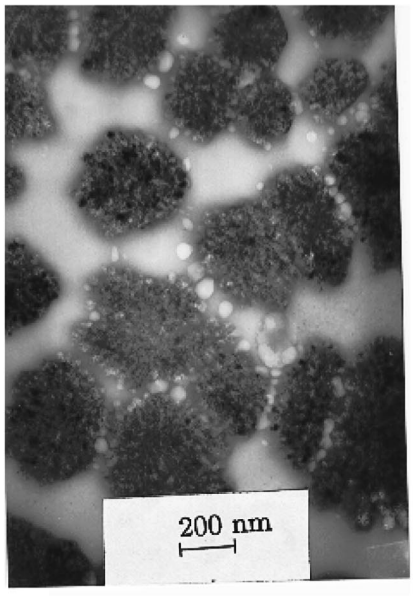

(a)

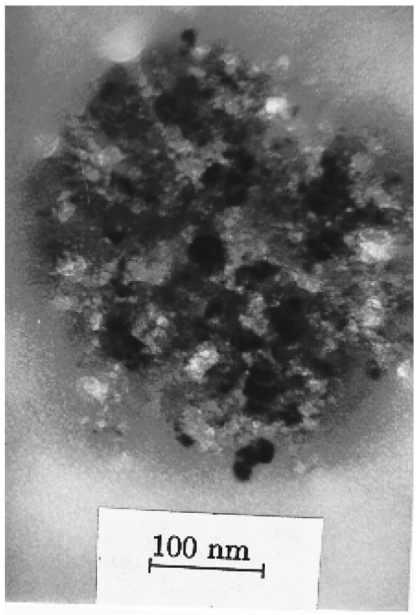

(b)

FIG. 7. (a) Cross linking in the clustered region shown in the bright field transmission electron micrograph of the PPO film implanted at a fluence of 1×10^{16} ions/cm^2, (b) amplified bright field transmission electron micrograph of the clustered region in PPO film implanted at 1×10^{16} ions/cm^2.

axis was found to be along $\langle 070\rangle$ direction. Micro-diffraction study of the matrix outside the clustered feature showed a broad, diffuse ring pattern (not shown in figure) indicating presence of amorphous phase in the matrix. Thus, the growth of single crystalline graphitelike carbonaceous clusters are confirmed to have been formed as an effect of ion-irradiation above a critical fluence of 1×10^{16} ions/cm^2.

Evidence for the formation of fractal patterns due to aggregation of small graphitelike clusters surrounded by an amorphous matrix in the N^+ beam-induced PPO films is pointed out in the above sections. The dimension of the fractal pattern was obtained using manual box counting. The area of coverage (A) as a function of radius (R) is given in Fig. 11 for the sample irradiated at a fluence of 5×10^{16} ions/cm^2. From the log-log plot in Fig. 10, it is seen

FIG. 8. Bright field transmission electron micrograph of the PPO film implanted at a fluence of 5×10^{16} ions/cm^2 showing the growth of larger fractal patterns containing carbonaceous clusters.

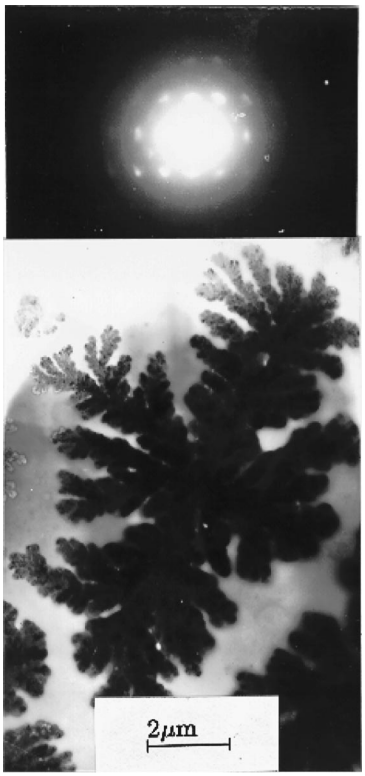

FIG. 9. Amplified bright field transmission electron micrograph of the PPO film implanted at a fluence of 5×10^{16} ions/cm^2. The crystalline microdiffraction pattern of the clustered region is shown in the outset. Zone axis of the spotted microdiffraction pattern is calculated to be $\langle 700\rangle$.

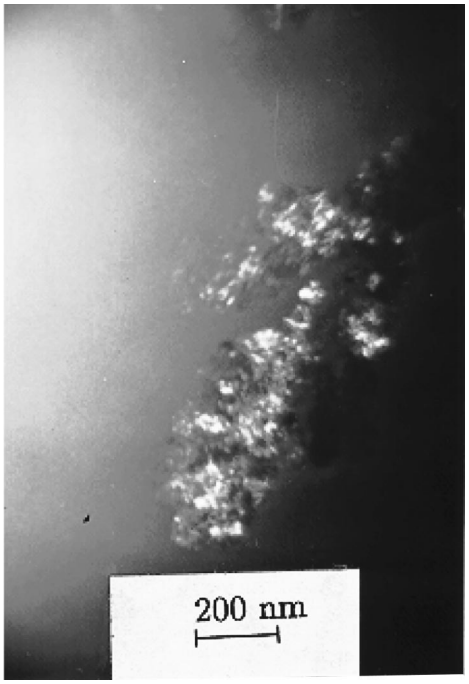

FIG. 10. Dark field transmission electron micrograph of the PPO film implanted at a fluence of 5×10^{16} ions/cm^2.

that A is proportional to R^D, where D is the dimension of the fractal. The value of D is found to be 1.37 ± 0.02 (Fig. 11). This value is comparable to the fractal dimensions of 1.30 ±0.075 for the two-dimensional growth of clusters as simulated by Meakin for diffusion limited aggregation on fiber.[16]

C. Evidence for clusters from optical spectroscopy

In the UV-VIS-NIR spectra of N^+ beam-bombarded PPO films, the transmittance increased as a function of wave length indicating a resemblance to that in *a*-C:H. As the ir-

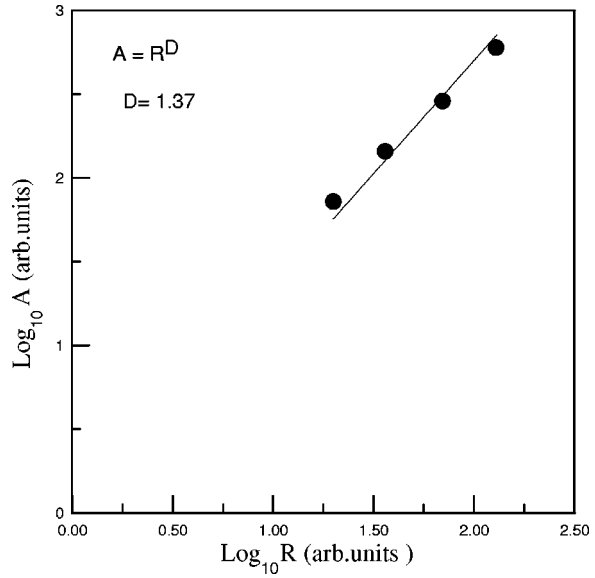

FIG. 11. Log-log plot for A vs R in determining the fractal dimension of the 100 keV N^+ implanted PPO film at a fluence of 5×10^{16} ions/cm^2.

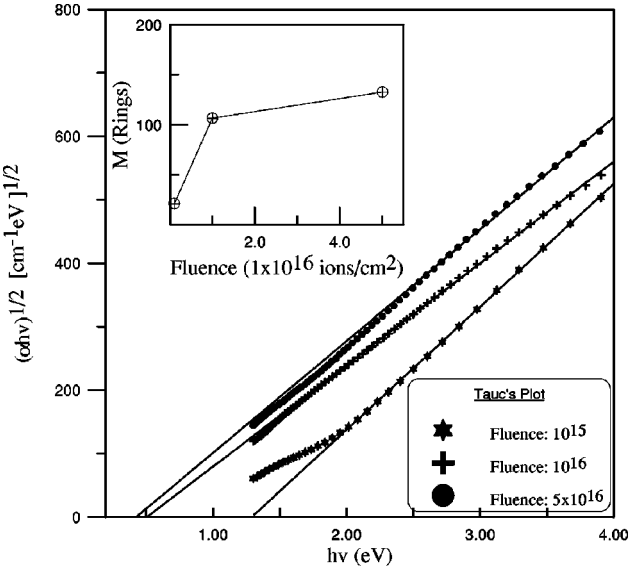

FIG. 12. Tauc's plot for determination of optical band gap of 100 keV N^+ implanted PPO films. Inset shows the increased number of ring formation as a function of fluence.

radiation dose increases, the absorption edge is found to shift towards the longer wave length.[23] The disorder in the irradiated films was estimated by us following Urbach equation[24] and the disorder parameter held a linear relationship with the calculated optical band gaps from the spectra.[23] Similar correlation is reported for *a*-C:H and *a*-Si:H.[24,25] Tauc's formula is widely used to determine the optical band gap for amorphous and carbonaceous materials. Figure 12 shows the Tauc's plot for N^+ beam-irradiated PPO films for the fluence in the range of $10^{15}-5\times10^{16}$ ions/cm^2. It is obvious that a progressive decrease in the band gap from 1.5 to 0.45 eV is observed as a function of fluence. The Tauc's effective optical gap value of the implanted films may be used to characterize their short and medium range order. In particular, sizes of the graphitelike (sp^2 bonded) regions may be estimated. This issue has been reported in detail by Robertson and O'Reilly.[10] They proposed that the Tauc's edge of fundamental optical absorption of amorphous carbon, E_g, can be correlated by the equation:

$$E_g=\frac{2\beta}{M^{1/2}},$$

where M is the number of six member rings that constitute the sp^2-bonded fragments; $\beta=-2.9$ eV is a constant, more specifically, is the nearest-neighbor interaction between the π orbitals of six member rings. Thus, a progressive increase in the average size of the clusters as a function ion fluence is inferred from the above relation. The number of fused rings calculated using the above relation, are plotted with the varying fluence (inset of Fig. 12). Therefore, UV-VIS-NIR analysis is consistent with the ion beam-induced agglomeration, through which the aromatic rings obtain a new stable state. The drastic decrease of E_{g} with fluence ranging from 1×10^{15} to 1×10^{16} ions/cm^2 suggests the transformation from separated aromatic rings to a structure similar to graph-

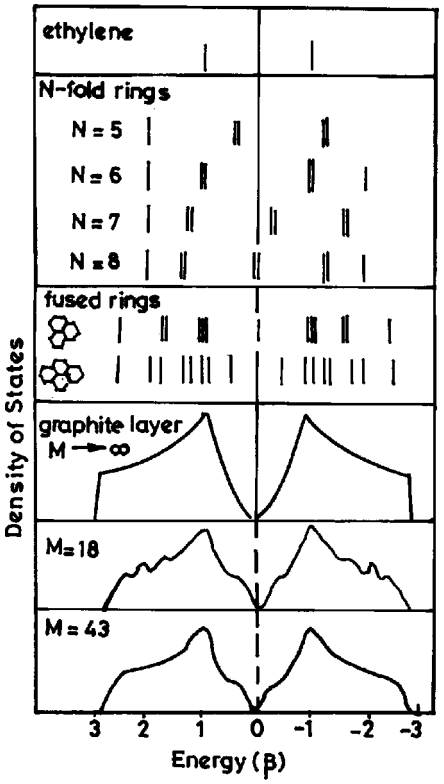

FIG. 13. The density of state (DOS) vs energy plot for various fused rings and the same is compared with graphitic layer (according to Ref. 21).

ite. Similar kind of observations were reported in case of B^+ beam-irradiated polyimides films.[26]

The duration that bombarded ions come to stop in the surface layer and get dissipated into the matrix is approximately 10^{-10} s; consequently, the structural transformation produced by ion irradiation cannot be definitely governed by conventional equilibrium thermodynamic. Liu *et al.*[27] suggested that the structural similarity, which leads to the readiness of structural transformation, plays a much more important role than the thermodynamic factors during the ion beam-induced transformation in solids. Therefore, from this standpoint, the conversion from aromatic rings into hexagonal graphite cells under ion irradiation is also considered to be favorable. This is due to the existence of their high degree of structural similarity such as bond length and planar hexagonal symmetry in both the systems. Upon ion irradiation, the originally isolated aromatic rings could condense into the clusters of aromatic rings, and then form graphitelike structure.

The graphitelike nature of the clusters present in a-C:H structure was confirmed through Hueckel molecular orbital calculations considering only the π interactions of the planar sp^2 sites of the ring with minimum coupling between the σ and π states.[21] The π binding energies and the electronic spectra of a wide range of possible structure were calculated by Robertson[21] and are shown in Fig. 13 along with the spectrum of graphite. The density of state (DOS) of finite layers of fused benzene rings with number of rings, $M=18$ already resembles that of a graphite layer with $M\rightarrow\infty$ and by $M=43$, the spectrum is smooth. π bonding strongly favors aromatic rings over olefinic chains with a preference for clustering of the former to graphitic sheets. Thus fused sixfold rings are a preferred configuration for the ion beam-induced formation of clusters.

As discussed earlier, ion-irradiated polymer show precipitation of either graphitelike (GLC) or diamondlike (DLC) carbonaceous particulate depending on the predominant role of either electronic or nuclear energy loss of the ions. In this model, Wang *et al.*[1] have assumed a critical transition temperature above which the thermodynamic relaxation process will form the graphite structure, below which thermodynamic relaxation process behaves like a nonthermodynamic process to form an amorphous carbon or diamondlike structure. They mentioned that in case of 180 keV As^+ ion on polyamideimide (PAI), the electronic energy stopping power 300 eV/nm, which was found much less than the critical energy stopping power $\sim 3.4\times 10^3$ eV/nm calculated for critical temperature. Therefore, the graphitelike structure formation was ruled out for 180 keV As^+ ion irradiation on PAI. In our case, calculation for 100 keV N^+ ion interaction with PPO using TRIM90 code,[20] showed that the electronic energy loss ($\sim$300 eV/nm) is six times more than the nuclear energy loss ($\sim$50 eV/nm). However, we find the formation of graphitelike clusters in the 100 keV N^+ ion-irradiated PPO films beyond the fluence of 1×10^{15} ions/cm^2 as analyzed from TEM and FT-Raman studies. The possible explanation for graphitelike cluster formation from the critical temperature model may be argued from the point of view that at high fluence, the time interval of consecutive ions through the same region of material will probably be comparable to or even smaller than the lifetime of the transient temperature pulse. The net temperature, Wang *et al.*[1] argued, of this region may reach the critical temperature required to create the graphitic structure. Thus, presence of graphitelike carbonaceous particles in the ion-irradiated PPO at high fluences ($\geqslant 1\times 10^{15}$ ions/cm^2) can be realized from this standpoint.

The growth process of ion-induced fractal patterns in polymer films seems to follow the diffusion limited deposition on fibers, as proposed by Meakin[16] using Monte Carlo simulations. In his model, a particle is introduced in the neighborhood of the fiber and allowed to diffuse by a series of jumps and eventually gets attached to the fiber. The procedure is repeated many times until a sufficiently large deposit has been grown on the fiber. The fragmented polymer molecules, as well as, the cross-linked materials as an effect of ion-irradiation are reported[11] to posses fibrous structure, which in turn may help in aggregation of nanosized single crystalline graphitic particles in a fractal pattern according to DLA model proposed by Meakin.[16] In the present case, we find the growth of the fractal patterns for a wide range of fluences owing to a large magnitude of energy deposition culminating in precipitation of carbonaceous clusters, which in turn, agglomerate in the fractal pattern.

IV. CONCLUSIONS

The Raman spectral studies and the TEM images evidence the presence of two distinct phases in the implanted PPO film: an amorphous matrix and a single crystalline cluster phase. At a larger ion fluence, the nanosized crystalline

clusters increase in size and in number density. Microbeam diffraction patters of these clusters indicate their structure to resemble the crystalline graphitic structure with zone axis along $\langle 070 \rangle$ direction. The evolution of graphitic clusters are supported by the FT-Raman and UV-VIS spectroscopic results. The aggregation of these clusters forms fractal patterns, which shows a dimensionality of 1.37 ± 0.02 indicating possible DLA model for cluster growth.

ACKNOWLEDGMENTS

The authors are grateful to Saroja Sai Baba for her help in performing the TEM studies. We also thank M. Vijaylakshmi for useful discussions while preparing the manuscript. One of us (A.D.) acknowledges Inter-University Consortium–Department of Atomic Energy Facility (IUC-DAEF) for financial support.

[1] Y. Q. Wang and R. E. Giedd, Nucl. Instrum. Methods Phys. Res. B **79**, 659 (1993).
[2] T. Venkatesan, S. R. Forrest, M. L. Kaplan, C. A. Murray, P. H. Schmidt, and B. J. Wilkens, J. Appl. Phys. **56**, 2778 (1984).
[3] D. Fink, K. Ibel, P. Goppelt, J. P. Biersack, L. Wang, and M. Behar, Nucl. Instrum. Methods Phys. Res. B **46**, 342 (1990).
[4] O. Yu. Posudievsky, Radiat. Eff. Defects Solids **137**, 119 (1995).
[5] D. Xu, X. L. Xu, and S. C. Zou, Mater. Lett. **12**, 12 (1991).
[6] E. Adem, M. Avalos-borja, J. Rickards, and R. Trejo-luna, Radiat. Phys. Chem. **48**, 727 (1996).
[7] J. Davenas, P. Thevenard, G. Boiteux, M. Fallovier, and X. L. Lu, Nucl. Instrum. Methods Phys. Res. B **46**, 317 (1990).
[8] D. Fink, W. H. Chung, R. Klett, A. Schmoldt, J. Cardoso, R. Montiel, M. H. Vazquez, L. Wang, F. Hosoi, H. Omichi, and P. Goppelt-Langer, Radiat. Eff. Defects Solids **133**, 193 (1995).
[9] G. Compagnini and R. Reitano, Surf. Interface Anal. **22**, 520 (1994).
[10] J. Robertson and E. P. O'Reilly, Phys. Rev. B **35**, 2946 (1984).
[11] G. R. Rao, Z. L. Wang, and E. H. Lee, J. Mater. Res. **8**, 927 (1993).
[12] G. Foti and R. Reitano, Nucl. Instrum. Methods Phys. Res. B **46**, 306 (1990).
[13] M. L. Kaplan, S. R. Forrest, P. H. Schmidt, and T. Venkatesan, J. Appl. Phys. **55**, 732 (1984).
[14] B. Wasserman, Phys. Rev. B **34**, 1926 (1986).
[15] T. A. Witten and L. M. Sander, Phys. Rev. Lett. **47**, 1400 (1980); Phys. Rev. B **27**, 5686 (1983).
[16] P. Meakin, Phys. Rev. A **27**, 2616 (1983).
[17] L. J. Huang, J. R. Ding, H.-D. Li, and B. X. Liu, J. Appl. Phys. **63**, 2879 (1988).
[18] A. Das, G. Ghosh, S. Dhara, and A. Patnaik, Mater. Lett. **38**, 82 (1999).
[19] A. Das, C. Mukundan, B. Sundarakkannan, S. Dhara, and A. Patnaik, in *Laser Application in Material Science and Industry*, edited by R. Kesavamurthy, Akhilesh K. Arora, C. Babu Rao, and P. Kalyansundaram (Allied Publisher, India, 1997), p. 118.
[20] J. P. Biersack and L. G. Haggmark, Nucl. Instrum. Methods **174**, 257 (1980).
[21] J. Robertson, Adv. Phys. **35**, 317 (1986).
[22] D. Beeman, J. Silverman, R. Lynds, and M. R. Anderson, Phys. Rev. B **30**, 870 (1984).
[23] A. Das, S. Dhara, and A. Patnaik, Nucl. Instrum. Methods Phys. Res. B **149**, 53 (1999).
[24] G. D. Cody, T. Tiedje, B. Ables, B. Brooks, and Y. Goldstein, Phys. Rev. Lett. **47**, 1480 (1981).
[25] Fangqing Zhang, Bailian Ma, and Guanghua Chen, Mater. Lett. **12**, 63 (1991).
[26] X. L. Xu, D. Xu, H. L. Xu, R. Wang, S. C. Zou, G. D. Du, and G. Q. Xia, J. Vac. Sci. Technol. A **12**, 3200 (1994).
[27] B. X. Liu, X. Zhou, and H. D. Li, Phys. Status Solidi A **113**, 11 (1989).